JOURNAL OF GEOPHYSICAL RESEARCH, VOL. 115, B04409, doi:10.1029/2009JB006287, 2010

Reexamination of the present stress state of the Atera fault system, central Japan, based on the calibrated crustal stress data of hydraulic fracturing tests obtained by measuring the tensile strength of rocks

Futoshi Yamashita,[1] Kazuo Mizoguchi,[1] Eiichi Fukuyama,[1] and Kentaro Omura[1]

Received 5 January 2009; revised 11 November 2009; accepted 23 November 2009; published 23 April 2010.

[1] To investigate past faulting activity and the present physical state of intraplate faults in Japan, we reexamined the crustal stress measured by hydraulic fracturing tests (HFTs) incorporating the tensile strength of rocks. The tensile strength was measured by fracturing hollow cylindrical rock samples which were obtained close to the Atotsugawa, the Atera, and the Rokko-Awaji fault systems in central Japan, where in situ stress measurements had been conducted with HFTs. The measured tensile strength data reveal that the reopening pressure was obviously biased in the conventional HFT with a large compliance system. We reestimated the reopening pressure using the measured tensile strength and recalculated the in situ stress around the Atera fault system. We found that the shear stress decreases toward the fault. Although the past long-term slip direction of the Atera fault system has been considered to be left-lateral from the geomorphological features, the reestimated stress suggests that the present slip direction is right-lateral, a finding that is also supported by the present-day horizontal crustal deformation observed by triangulation and GPS surveys. The amount of accumulated right-lateral dislocation estimated from the stress data using the dislocation model of Okada (1992) was 2.1 m. Because the current slip rate from the GPS survey is 1.9 ± 1.4 mm/yr, the accumulation period of the right-lateral dislocation becomes approximately 1100 ± 800 years if the slip rate is stable. This estimation suggests that during the latest earthquake the Atera fault system underwent right-lateral dislocation.

Citation: Yamashita, F., K. Mizoguchi, E. Fukuyama, and K. Omura (2010), Reexamination of the present stress state of the Atera fault system, central Japan, based on the calibrated crustal stress data of hydraulic fracturing tests obtained by measuring the tensile strength of rocks, *J. Geophys. Res.*, *115*, B04409, doi:10.1029/2009JB006287.

1. Introduction

[2] The total value of in situ crustal stress is a significant index for understanding the mechanism of earthquake occurrence and its relation to the tectonic background. The hydraulic fracturing test (HFT) is a powerful technique for measuring the total stress in the crust. The HFT has been commonly conducted for a long time in many parts of the world [e.g., *Zoback*, 1992]. In particular, this is the only technique currently available to conveniently measure the stress at great depths because the procedure is quite simple and can be performed at the bottom of a deep borehole. The conventional HFT procedure is as follows [*Haimson and Cornet*, 2003]: A straddle packer is installed in a drilled borehole and is positioned at the depth where the measurement is to be conducted. The tested interval is sealed off, and water is injected into it while the pressure and flow rate of the injected water are measured. When the tensional stress due to the water pressure overcomes the sum of the tensile strength and the compressional stress on the borehole wall in the direction of the horizontal maximum stress, fractures are initiated, and the water pressure rapidly decreases because of the leakage of water through the fractures. This peak pressure that induces fracture initiation is called the "breakdown pressure" (P_b). The pump is stopped, and the water pressure continues to decrease until the fractures close. The pressure at which the fractures close is called the "shut-in pressure" (P_s). The water is injected again, and the pressure slope bends when the water pressure exceeds the compressional stress and the fracture is reopened. The pressure at which the fractures reopen is called the "reopening pressure" (P_r). The azimuths of fractures are measured with the impression packer after several repeats of the above procedures. From the basic equation of HFT, P_r and P_s can be expressed as follows [e.g., *Kehle*, 1964]:

$$P_r = 3S_{hmin} - S_{Hmax} - P_p$$
$$P_s = S_{hmin} \quad (1)$$

[1]National Research Institute for Earth Science and Disaster Prevention, Tsukuba, Japan.

0148-0227/10/2009JB006287

where S_{hmin}, S_{Hmax}, and P_p represent the horizontal minimum principal stress, horizontal maximum principal stress, and pore pressure, respectively. The National Research Institute for Earth Science and Disaster Prevention (NIED) conducted several in situ stress measurements near the intraplate active fault to estimate the stress acting on the fault [e.g., *Ikeda et al.*, 2001, 2002]. One important application of the stress measurement data is the modeling of earthquake faulting. *Yamashita et al.* [2004] estimated the fault strength of the Nojima fault at a shallow depth using the in situ stress data measured at several places around the Rokko-Awaji fault system just after the 1995 Kobe earthquake.

[3] Although knowing the stress is quite useful as mentioned above, it has been suggested recently that the reopening pressure, which is one of the parameters used to determine stress values, might not have been measured correctly in HFT since many reports have found that two independent parameters, the reopening pressure and the shut-in pressure, are similar [e.g., *Lee and Haimson*, 1989; *Sano et al.*, 2005]. *Ito et al.* [1999] clarified this problem using numerical simulation analysis. In their simulation, the pressure change due to the reopening of the fracture is so tiny that the corresponding pressure change cannot be recognized in the pressure curve. They also claimed that the reopening pressure should be measured using a system with small compliance, i.e., a system that requires only a very small amount of water to increase the water pressure. If the tensile strength of the rock (T) is available, however, it becomes possible to estimate the reopening pressure more accurately based on the following relation:

$$P_r^{'} = P_b - T \tag{2}$$

where we define the reopening pressure estimated from equation (2) as P'_r. Note that this relation can only be applied to impermeable rocks like granite because the percolation effect that is not taken into account in equation (2) becomes critical in permeable rocks [e.g., *Schmitt and Zoback*, 1989]. Since the rock samples used in this study were granite or gneiss, as shown later, this equation can be used in this study. It should also be noted that, strictly speaking, the physical meaning of P'_r is not "reopening pressure" but "the first opening pressure." However, we refer to it as "reopening pressure" in this study since using a different name may give rise to unnecessary confusion. Because of the uncertainty in determining the reopening pressure, International Society for Rock Mechanics (ISRM) recommends that the tensile strength be measured to obtain more accurate stress data, though ISRM also introduced the use of P_r as an alternative method when the tensile strength is not available [*Haimson and Cornet*, 2003].

[4] The main purpose of this paper is to reexamine the in situ stress data obtained in past experiments [e.g., *Ikeda et al.*, 2001, 2002] using the tensile strength of the rock, which is an independent observable in the experiments. For this purpose, we constructed a new apparatus to measure the tensile strength of rock samples. After calibrating the tensile strength using Inada granite, we measured the rock samples taken at boreholes near the Atotsugawa, Atera, and Rokko-Awaji fault systems where HFT had been conducted. In particular, we will show the results of reexamining the present activity of the Atera fault system using reliable stress data.

2. Measurement of Tensile Strength

2.1. Measurement Method for Tensile Strength

[5] Tensile strength is a basic property of rock, and many measurement methods have been proposed [*Jaeger and Cook*, 1969]. The most common method is the Brazilian test, in which a disk-shaped sample is uniaxially compressed, and the tensile strength is estimated from the pressure applied to the fracture. Although this method is convenient and thus advantageous for measuring a large number of samples, it does not simulate the conditions of in situ HFT [*Haimson and Cornet*, 2003]. The direct pull test enables us to conduct the measurement under a theoretical tensile stress condition. However, it should be noted that in this test uniform and uniaxial stress is applied at the center of a cylindrical sample without applying torsion or moment to the sample. This makes it difficult to fix the sample to the jig of the testing machine.

[6] In order to measure the tensile strength of rock reliably and accurately, we selected a laboratory HFT in which a cylindrical hollow rock sample is fractured by pressurizing the wall inside the sample. This method is recommended by ISRM since the stress condition is similar to that of in situ HFT [*Haimson and Cornet*, 2003]. To conduct this measurement, we made an apparatus consisting of a water pump, mechanical packer, sample holder, and pressure sensor (Figures 1a and 1b). We used a cylindrical rock sample with a cylindrical hole at the center parallel to the core axis. The diameter of the hole was set at 25 mm to avoid any size effect of the hole. This selection of the diameter was derived from the experimental results of *Haimson and Zhao* [1991], who investigated the effect of borehole size on the breakdown pressure. They conducted laboratory HFT using granite and limestone with diameters of 3.2–50.8 mm and concluded that the data for samples with a hole diameter of more than 20 mm were stable and directly usable in the in situ HFT. The experimental results were also introduced by *Cuisiat and Haimson* [1992]. We set the packer interval to 50 mm, which corresponds to the pressurized length of the sample. To achieve a similar condition as in the in situ HFT, we saturated all core samples with water by placing them in water inside a vacuum vessel for 72 h. The water pressure was measured by a strain gauge-type pressure sensor. The signal was processed by the signal conditioner and recorded by a personal computer at a frequency of 1 kHz with 24-bit resolution. By pouring water at a constant rate of 10 mm^3 min^{-1}. into the core sample hole, which was sealed by the mechanical packer (Figure 1c), we monitored the water pressure. The pressure increased as time passed, which increased the tensional stress at the inner wall of the rock sample. Then, when water pressure overcame the tensile strength and water began to leak from the initiated fracture, the pressure decreased rapidly, and a fracture was observed in the rock sample. This peak pressure is related to the tensile strength of the sample. Typical behavior of the pressure during the experiment is shown in Figure 2. The

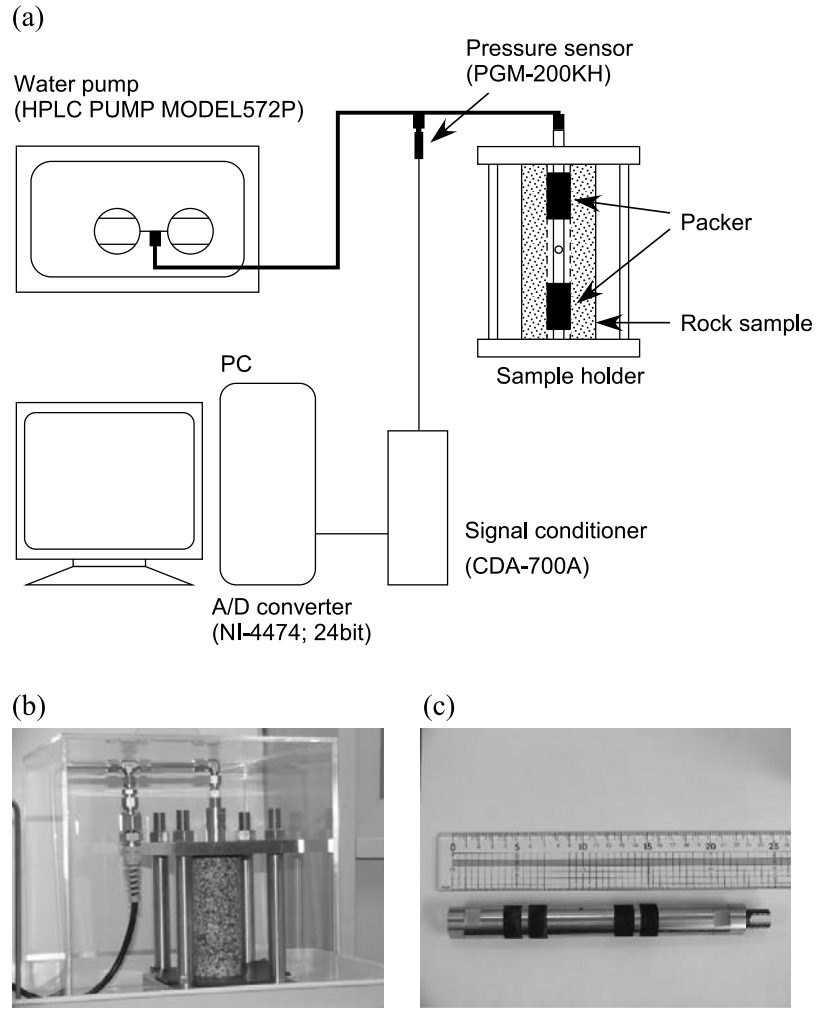

Figure 1. (a) Schematic diagram of the system for measuring the tensile strength of a hollow cylindrical core sample. The inner hole of the sample is sealed by a mechanical packer and is pressurized by water until a fracture occurs. The pump sends the water into the rock sample, and a strain gauge type pressure sensor with a signal conditioner measures the pressure. The signal was acquired with a 24-bit 1 kHz A/D converter equipped in PC. (b) Photograph of the sample holder, sample, and packer. (c) Photograph of the mechanical packer. By shortening the inner tube, black rubber tubes shrink and seal the inner hole of the rock sample.

tensile strength of the rock (T) can be estimated by the following equation [*Jaeger and Cook*, 1969]:

$$T = P_i\left(R_2^2 + R_1^2\right)/\left(R_2^2 - R_1^2\right) \quad (3)$$

where P_i is the peak pressure observed in the experiment and R_1 and R_2 are the inner and outer radii of the sample, respectively.

2.2. Calibration Test Using Inada Granite

[7] Although a laboratory HFT is the best way to obtain the tensile strength of rock in order to correct the in situ conventional HFT data, the reliability of the apparatus used for the measurement should be verified before the main test. For this reason, we conducted a calibration test using core samples of Inada granite, the physical properties of which are well known [e.g., *Lin*, 2002; *Takemura and Oda*, 2005; *Fujii et al.*, 2007]. Inada granite has three orthogonal planes, known as the "rift" (r-), "grain" (g-), and "hardway" (h-) planes, along which fracture tends to occur. The tensile strength is weakest on the r-plane, strongest on the h-plane, and of intermediate strength on the g-plane. We prepared three sets of three Inada granite samples whose core axes are perpendicular to either the r-, g-, or h-plane. In total, we prepared nine samples. The sample length was 140 mm, and its outer diameter was 60 mm. Table 1 shows the results of the calibration test. In all cases, a fracture occurred along the weakest plane along the core axis; the fracture occurred on the r-plane in six samples, on the g-plane in three, and on the h-plane in none. In Table 2, the tensile strengths of Inada granite estimated by the Brazilian test and the uniaxial pull test are compared [*Fujii et al.*, 2007; *Lin et al.*, 2008]. The tensile strengths estimated by the Brazilian tests and the pull tests are similar to those estimated in the present study. In addition, the measurement errors show that the reproducibility of our measurements is comparable to that of pull

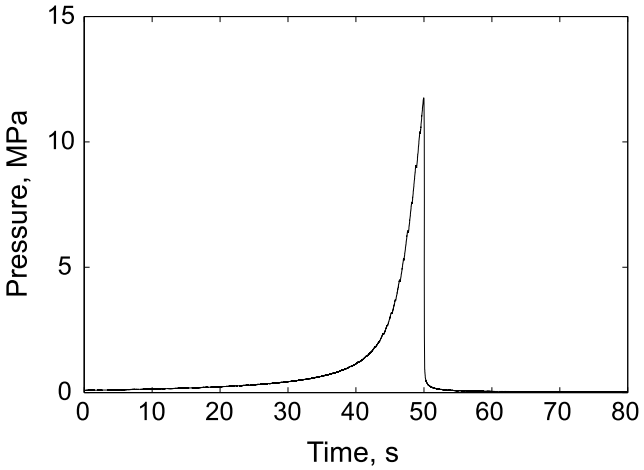

Figure 2. A typical example of pressure change during a test. A fracture occurred at about 50 s. The peak pressure was used for the estimation of tensile strength.

tests and superior to that of Brazilian tests. From the results of the calibration test, we concluded that our measurements are sufficiently reliable.

2.3. Description of Core Samples

[8] NIED conducted several in situ stress measurements near the active fault systems in central Japan. The locations included Atotsugawa (ATG) well near the Atotsugawa fault system; Ueno (UEN), Fukuoka (FUK), and Hatajiri (HTJ) wells near the Atera fault system; and Hirabayashi (HRB), Iwaya (IWY), and Kabutoyama (KBY) wells near the Rokko-Awaji fault system (Figures 3 and 4). We used a total of 32 core samples obtained at these boreholes where the stress measurement by the HFT had been conducted. The detailed features of these core samples are described in Table 3. The length and outer diameter of the samples ranged between 139.1 and 140.1 mm and between 55.1 and 101.5 mm, respectively. To measure the tensile strength during the HFT, the core samples had to be taken exactly where the HFT was conducted. Thus we collected the samples from locations as close as possible to the corresponding HFT depths. When cores close to the HFT depth were not available, we carefully selected cores at other depths whose physical properties were considered to be similar by consulting the physical well logging data. Figure 5 shows photographs of the core samples of three representative rocks: fine-grained Granite (IWY_A_1), middle-grained Granite (UEN_A_1), and Gneiss (ATG_A_1). The maximum grain sizes of IWY_A_1, UEN_A_1, and ATG_A_1 were approximately 1, 3, and 6 mm, respectively. The tensile strength data measured here inevitably contain some errors caused by the measurement itself and due to small variations in physical properties between samples. Thus we measured the tensile strength for three core samples and obtained tensile strength data by averaging these values.

2.4. Tensile Strength of Core Samples

[9] Although we prepared 32 samples for the tests, we could not measure the tensile strength for 13 samples due to the outflow of pressurized water from preexisting fractures. These fractures were so tiny that we could not recognize them by eye, but as the water pressure was increased during the test, water started to flow from the samples through these tiny fractures. The 13 failed samples were collected from deeper boreholes around the Rokko-Awaji fault system (HRB_A_1–3, IWY_A_1–4, KBY_A_1–3, KBY_B_1–3). Generally, the horizontal stress increases with the depth. The release of high horizontal stress from rock by drilling often gives rise to new fractures, e.g., core disking [e.g., *Amadei and Stephansson*, 1997]. The failure of the laboratory HFTs with respect only to samples from great depths (>634 m) suggests that the fractures were generated due to the release of in situ stress during the collection of the samples. If such fractures are generated in situ, they are usually easy to recognize by eye due to the precipitation of minerals on the surface of the fracture. Ultimately, we obtained tensile strength data for 19 samples as shown in Table 4. Since we averaged the three measured values to obtain the tensile strength, the total number of tensile strength values obtained was seven. It should be noted that the tensile strength at the Iwaya well likely includes greater error because only one value from the sample IWY_A_5 was available. However, since the errors of each tensile strength value seem to be small compared with the field data, we hereafter neglect the errors.

[10] In Table 5, we show the results of the in situ estimation of crustal stress by conventional HFT in the wells drilled near the Atotsugawa, Atera, and Rokko-Awaji fault systems [*Ikeda et al.*, 2001, 2002]. The stress data near the Atotsugawa fault system were obtained in 2006 by the authors. There are 13 stress measurements in total that can be compared with the tensile strength data measured below. Using P'_r estimated by equation (2), we reestimated the horizontal maximum principal stress (S'_{Hmax}) using equation (1). It should be noted that S'_{Hmax} becomes less than S_{hmin} for RKA_1 in Table 5, which is apparently inconsistent with

Table 1. Result of Tensile Strength Measurements of Inada Granite

Sample ID	Tensile Strength, MPa	Average Tensile Strength, MPa	Fracture Plane
IND_H_1	7.4	6.7 ± 0.6	R
IND_H_2	6.4		
IND_H_3	6.4		
IND_G_1	6.0	6.2 ± 0.2	R
IND_G_2	6.4		
IND_G_3	6.1		
IND_R_1	8.3	8.4 ± 0.2	G
IND_R_2	8.6		
IND_R_3	8.3		

Table 2. Tensile Strength of Inada Granite Estimated by a Brazilian Test, Uniaxial Pull Test, and Our Test[a]

Measurement Plane	This Study	Uniaxial Pull Test		Brazilian Test
		Fujii et al. [2007]	*Lin et al.* [2008]	*Lin et al.* [2008]
R	6.5 ± 0.5	3.99–4.53	4.34 ± 0.25	4.34 ± 1.11
G	8.4 ± 0.2	6.61–7.13	7.92 ± 0.51	8.38 ± 1.98
H	-	7.85–8.74	7.09 ± 0.34	8.45 ± 1.48

[a]Errors represent 1σ (standard deviation). Tensile strength is measured in MPa.

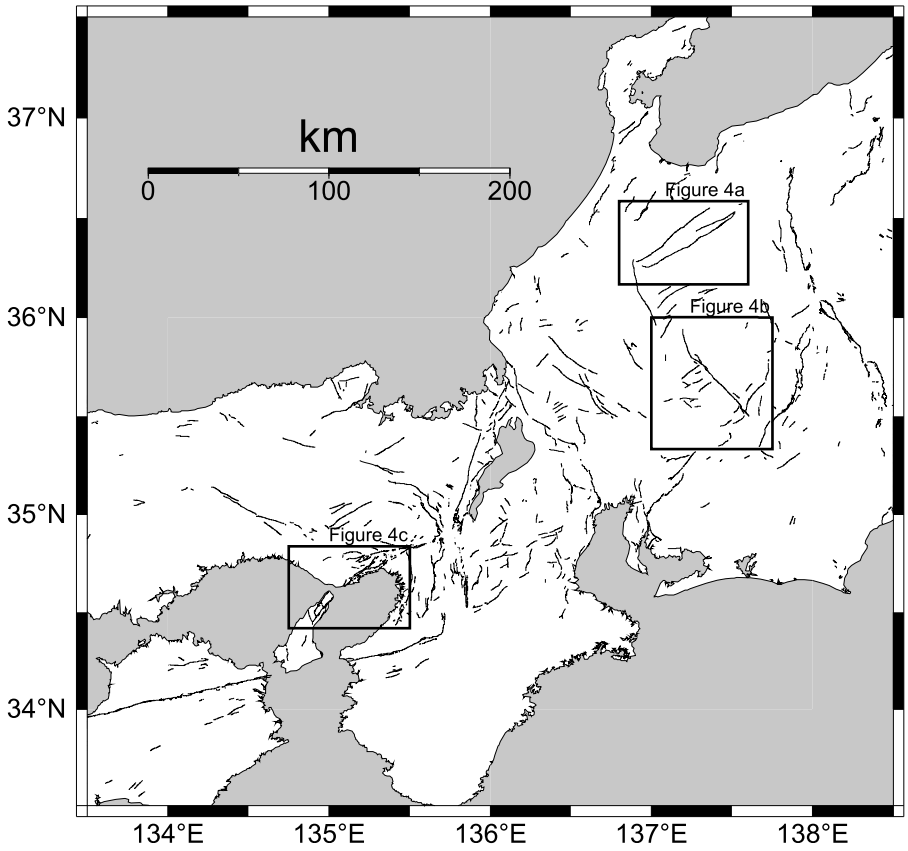

Figure 3. Map showing the surface traces of the active faults in central-southwest Japan. Stress data measured near the fault systems in the area enclosed by solid lines were reexamined in this study.

its definition. This suggests that for the case of RKA_1, the in situ HFT might not have been conducted appropriately owing to technical problems. Figure 6 compares P_r with P'_r as a function of P_s, excluding the data for RKA_1. This figure reveals that P_r is almost equal to P_s, and all of P_r is larger than P'_r. This means that P_r is biased. Here, if we assume that the in situ tensile strength is overestimated by the laboratory tensile strength, P_r also becomes greater than P'_r according to the definition in equation (2). However, this assumption cannot explain why P_r becomes similar to P_s. Since the size effect of the borehole can be neglected when the diameter is greater than 20 mm as mentioned earlier, the difference in tensile strengths between the in situ and laboratory measurements may also be neglected. Therefore as claimed by *Ito et al.* [1999], P_r obtained by the conventional method was inappropriately equal to P_s. See also the auxiliary material for a comparison between P_r and P'_r on the pressure-time curves.[1]

3. Reexamination of the Atera Fault System Activity

[11] The use of the tensile strength to reevaluate the above stress data enables us to estimate the stress state around the fault and the past faulting activity. Since there are a sufficient number of available stress data near the Atera fault system, we reinvestigated its present state of stress. The Atera fault system, with a length of 60–70 km, is located in central Japan and is trending approximately in the NW–SE direction as shown in Figure 4b. The predominant fault type is left-lateral strike slip, which is apparently revealed by the bending of rivers and the accumulated displacement observed in the terrace of the Kiso River [*Sugimura and Matsuda* 1965; *Tsukuda et al.*, 1993]. The slip rate is estimated from the accumulated dislocation to be about 2.8 mm/yr [*Tsukuda et al.*, 1993]. *Toda et al.* [1995] conducted a trenching survey to investigate the paleoseismicity of the Atera fault system. On the basis of the observation of the trench, they suggested that the latest event on the Atera fault system was the 1586 Tensho earthquake, and they estimated the recurrence interval as approximately 1800 years. The present seismicity of small earthquakes around the Atera fault system, in particular along the southern part of the fault system, is very low.

[12] As seen in Figure 4b, the stress measurements near the Atera fault system were conducted in three boreholes located on a line perpendicular to the surface fault trace. This arrangement of observation sites is conducive to elucidating the present state of the Atera fault system. It is expected that a regional stress around a fault would be distorted by a release of shear stress on the fault with coseismic and aseismic slips, and the distortion would depend on the distance from the fault as well as the amount and sense of the slip [e.g., *Hickman and Zoback*, 2004; *Townend and*

[1]Auxiliary materials are available in the HTML. doi:10.1029/2009JB006287.

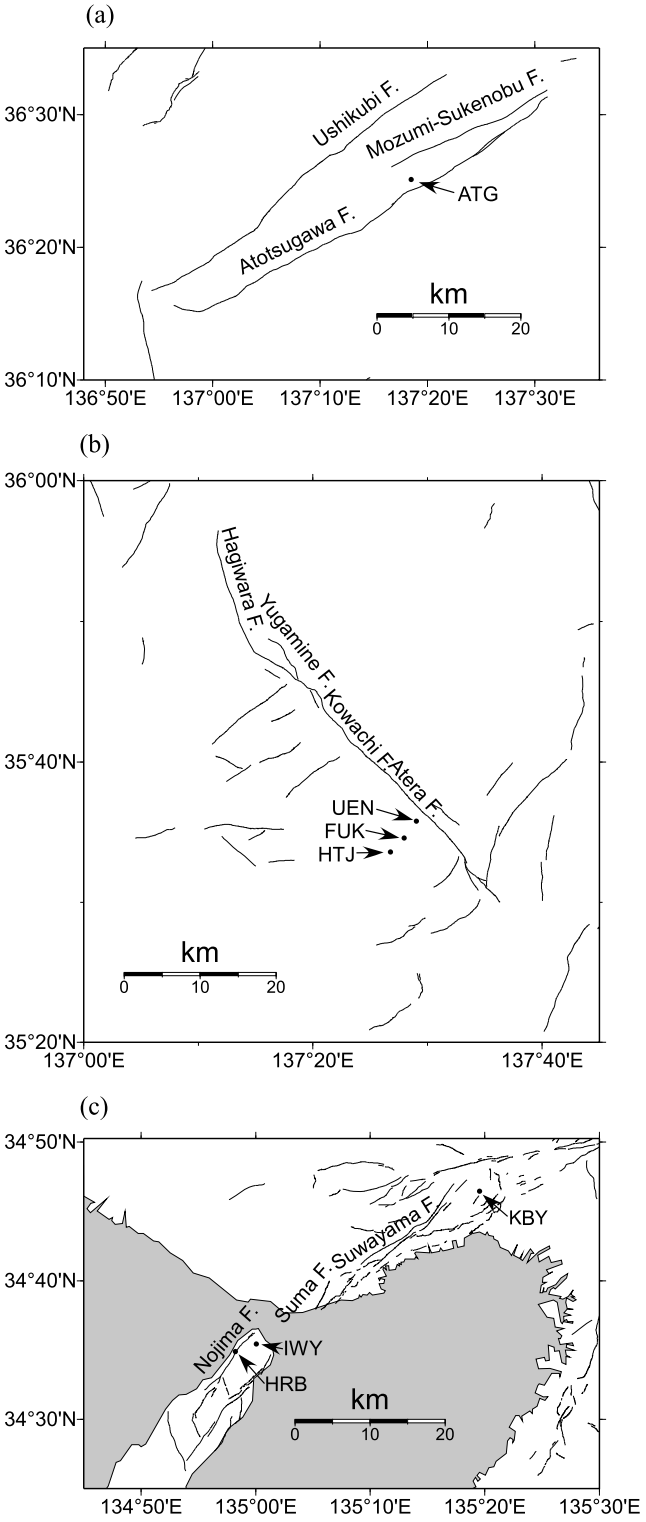

Figure 4. Maps showing the surface traces of (a) the Atotsugawa, (b) the Atera, and (c) the Rokko-Awaji fault systems. Solid circles show locations where the stress measurements were conducted.

Zoback, 2004]. Here we examine the shear stress around the fault system. Since the magnitude of shear stress typically depends on the depth, it should be normalized in order to compare the stress at different depths. Here, we introduce the r value, which is the horizontal maximum shear stress normalized by average stress as defined by $(S_{Hmax} - S_{hmin})/(S_{Hmax} + S_{hmin})$. This quantity indicates the minimum coefficient of friction on the plane where the maximum shear stress works without a pore pressure effect. If the stress field is uniform with a stress gradient proportional to the depth, r values are constant in the region. Figure 7a illustrates the relation between the r values calculated from the reestimated stress data and the distances from the boreholes to the Atera fault system. Figure 7a clearly demonstrates a decrease of shear stress near the fault. In contrast, no relations between the distances and the r values can be found in Figure 7b, where the r values are calculated using the in situ stress data obtained from the conventional HFT. Let us consider why r values become similar independent of location in Figure 7b. Following the numerical simulation by *Ito et al.* [1999], P_r intrinsically becomes equal to P_s, which immediately leads to the relation $S_{hmin} = (S_{Hmax} + P_p)/2$ from equation (1). If P_p is proportional to S_{Hmax}, S_{hmin} is also proportional to S_{Hmax} and can be written as αS_{Hmax}, where α is a constant. Substitution of this relation into the definition of the r value results in a constant r value independent of S_{Hmax} and S_{hmin} as follows: $r = (S_{Hmax} - \alpha S_{Hmax})/(S_{Hmax} + \alpha S_{Hmax}) = (1 - \alpha)/(1 + \alpha)$. Since horizontal stresses and pore pressure are basically depth dependent [e.g., *Brudy et al.*, 1997; *Lund and Zoback*, 1999; *Huenges et al.*, 1997] and thus the assumption that P_p is proportional to S_{Hmax} is generally acceptable, the estimation of in situ stress using the conventional P_r will seemingly lead to a similar r value at any location, even under varying stress conditions. This means that important tectonic characteristics of the crust are overlooked unless we use the stress data that have been reestimated using the tensile strength data.

[13] What causes the decrease in shear stress near the Atera fault system shown in Figure 7a? In order to answer this question, it is important to confirm whether stress accumulation due to tectonic loading has restarted since the previous earthquake. If the stress accumulation around the fault does not restart or if the accumulation is not sufficient, the decrease in shear stress near the fault would be caused by the stress drop that occurred during the previous earthquake. In this case, the fault strength may have sufficiently recovered, though it is difficult to confirm. If the stress accumulation has restarted, the stress heterogeneity near the fault would be caused by a successive release of shear stress due to dislocation of the fault, whose strength might not have recovered yet. Investigation of the present crustal deformation around the Atera fault system will help us to confirm which scenario is more credible. Figure 8 shows the horizontal crustal deformation rate estimated from continuous GPS observation over 5 years (June 2004 to June 2009) taken from the nationwide GPS network, GEONET (GPS Earth Observation Network System) provided by the Geographical Survey Institute (GSI) in Japan [*Hatanaka et al.*, 2003]. The analytical solution was the F3 solution. The location of site code 950284 is fixed in Figure 8, so the arrow represents the average displacement rate relative to the fixed site. Error ellipses reflect 1σ uncertainty. It seems that the southwestern side of the southern segment of the Atera fault system (970811, 020992, 940061, and 960616) moves to northwest in comparison with the northeastern side (020989 and 950274), though the displacement rates are

Table 3. Detailed Description of Core Samples Used for the Tensile Strength Measurements

Sample ID	Rock Type	Length, mm	Outer Diameter, mm	Inner Diameter, mm	Sampling Site	Sampling Depth, m
ATG_A_1	Gneiss	140.0	84.4	25.1	Atotsugawa fault system	9.72–10.0
ATG_A_2	Gneiss	139.9	84.3	25.1		10.42–10.68
ATG_A_3	Gneiss	137.0	84.3	25.1		10.88–11.02
FKO_A_1	Granite	140.0	56.1	25.1	Atera fault system(Fukuoka well)	131.45–132.00
FKO_A_2	Granite	140.0	55.9	25.2		131.45–132.00
FKO_A_3	Granite	140.0	56.2	25.2		131.45–132.00
FKO_B_1	Granite	140.0	62.9	25.2		261.00–261.50
FKO_B_2	Granite	139.7	62.9	25.2		261.00–261.50
FKO_B_3	Granite	140.0	62.9	25.2		261.00–261.50
HTJ_A_1	Granite	139.9	101.3	25.1	Atera fault system(Hatajiri well)	324.50–325.03
HTJ_A_2	Granite	140.0	101.5	25.2		324.50–325.03
HTJ_A_3	Granite	140.0	101.5	25.1		324.50–325.03
UEN_A_1	Granite	140.0	62.6	25.2	Atera fault system(Ueno well)	347.00–347.66
UEN_A_2	Granite	140.1	62.6	25.1		347.00–347.66
UEN_A_3	Granite	139.9	62.4	25.2		347.00–347.66
HRB_A_1	Granite	140.0	56.4	25.1	Rokko-Awaji fault system(Hirabayashi well)	1258.15–1258.62
HRB_A_2	Granite	140.0	56.3	25.2		1257.30–1257.61
HRB_A_3	Granite	140.0	56.3	25.2		1257.80–1258.30
HRB_B_1	Granite	140.0	56.8	25.1		451.55–451.83
HRB_B_2	Granite	140.0	56.7	25.0		451.83–452.39
HRB_B_3	Granite	140.0	56.7	25.1		451.83–452.39
IWY_A_1	Granite	139.1	55.1	25.1	Rokko-Awaji fault system(Iwaya well)	637.30–637.44
IWY_A_2	Granite	140.0	55.7	25.2		638.25–638.44
IWY_A_3	Granite	140.0	55.8	25.2		638.44–638.63
IWY_A_4	Granite	139.9	56.1	25.1		648.40–648.75
IWY_A_5	Granite	140.0	56.3	25.2		648.40–648.75
KBY_A_1	Granite	140.0	56.4	25.1	Rokko-Awaji fault system(Kabutoyama well)	802.2–802.75
KBY_A_2	Granite	140.0	56.2	25.1		802.2–802.75
KBY_A_3	Granite	140.0	56.4	25.1		802.2–802.75
KBY_B_1	Granite	140.0	56.0	25.1		634.10–634.45
KBY_B_2	Granite	140.0	55.9	25.1		634.10–634.45
KBY_B_3	Granite	140.0	56.1	25.1		634.62–634.85

rather small. This suggests that the southern segment of the Atera fault system is dislocating right-laterally even now, whereas the past slip direction was considered to be left-lateral based on geological and geomorphological observation. The GPS survey also suggests that the second possibility is acceptable, though the first possibility cannot be denied.

[14] Other observations shown below also suggest that the present stress state around the Atera fault system causes a right-lateral slip in the fault. Figure 9 shows the principal axes of horizontal maximum stress, the principal axes of horizontal strain, and the P-axes of small earthquakes. The gray solid lines show the azimuth of the principal axes of horizontal maximum stress estimated from the in situ stress measurements. All are approximately trending in the N–S direction, suggesting a right-lateral dislocation of the Atera fault system. The crosses with red and blue lines show the principal axes of horizontal strain obtained from the triangulation survey performed by GSI for 111 years between 1883 and 1994 (available at http://www.gsi.go.jp/cais/HIZUMI-hizumi7.html). The red and blue lines represent extension and contraction axes, respectively. If we assume that the directions of the contraction axes are consistent with those of the principal axes of horizontal maximum stress, the horizontal strain data also support the idea of a right-lateral slip in the Atera fault system.

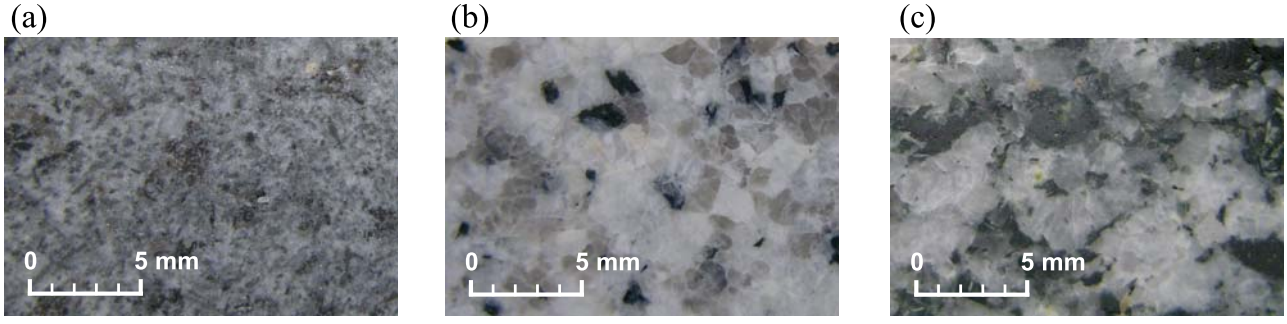

Figure 5. Photographs of three representative rocks in this study. (a) Granite sampled at Iwaya well near the Rokko-Awaji fault system. The maximum grain size is about 1 mm. (b) Granite sampled at Ueno well near the Atera fault system. The maximum grain size is about 3 mm. (c) Gneiss sampled at the Atotsugawa well near the Atotsugawa fault system. The maximum grain size is about 6 mm.

Table 4. Results of Tensile Strength Measurements[a]

Sample ID	Tensile Strength, MPa	Average Tensile Strength, MPa
ATG_A_1	15.0	14.6 ± 0.5
ATG_A_2	14.0	
ATG_A_3	14.8	
FKO_A_1	6.1	6.9 ± 0.7
FKO_A_2	7.2	
FKO_A_3	7.4	
FKO_B_1	6.2	6.3 ± 0.6
FKO_B_2	5.7	
FKO_B_3	6.9	
HTJ_A_1	11.5	12.1 ± 0.6
HTJ_A_2	12.0	
HTJ_A_3	12.7	
UEN_A_1	5.7	6.4 ± 0.8
UEN_A_2	6.2	
UEN_A_3	7.3	
HRB_B_1	7.6	9.3 ± 1.5
HRB_B_2	10.3	
HRB_B_3	10.0	
IWY_A_5	16.2	16.2

[a]Tests in which water leaked through the preexisting fracture before the pressure reached its tensile strength are excluded.

[15] The focal mechanism of a small earthquake is also a useful indicator of the regional tectonic stress. Unfortunately, seismicity around the Atera fault system is extremely low; F-net (a nationwide broadband seismograph network) operated by NIED determined only 29 focal mechanisms of earthquakes shallower than 20 km over a recent 10-year period (February 1998 to June 2008) in the region (Figure 9). F-net data are available at http://www.fnet.bosai.go.jp/freesia/top.php. In addition, the epicenter locations of these earthquakes were quite distant from the Atera fault system. Therefore these focal mechanisms cannot be an indicator of the stress field just near the Atera fault system but could be considered supplemental information. The P-axes of earthquakes (orange lines in Figure 9) are trending in the direction of WNW–ESE on average, and those directions seem to be inconsistent with the direction of horizontal compressional stress around the southern part of the Atera fault system. However, it seems that the directions of the contraction axes of horizontal strain vary from NNW–SSE in the south to NW–SE in the north, and they become similar to the directions of the P-axes in the northern region. Therefore it seems reasonable to consider that the regional stress varies with the location even within the region shown in Figure 9. These results also suggest that the northern segment of the Atera fault system (known as the Hagiwara fault) may be under the condition of left-lateral slip, whereas the slip direction of the southern segment (known as the Atera fault) changed from left- to right-lateral some time ago and is aseismically dislocating right-laterally at present. Differences in the faulting activity between the northern and southern segments of the Atera fault system were also suggested by the geological survey [*Toda et al.*, 1996], which shows that the two segments did not always dislocate simultaneously and that the Hagiwara fault did not move during the previous earthquake.

[16] Given that the southern segment of the Atera fault system is aseismically dislocating right-laterally, we evaluated the amount of accumulated dislocation. Here we assumed that the right-lateral dislocation on the Atera fault is the only cause of the decrease in differential shear stress (r value) near the fault (see Figures 10a and 10b). Therefore

Table 5. In Situ Stress Measurement Results With the Obtained Tensile Strength and the Corresponding Reopening Pressure and Horizontal Maximum Stress

				Data Estimated From in Situ Measurement					Data Estimated From in Situ Measurement and Tensile Strength		
Data ID	Fault System	Well	Depth, m	P_b, MPa	P_r, MPa	P_s, MPa	S_{Hmax}, MPa	S_{hmin}, MPa	T, MPa	P'_r, MPa	S'_{Hmax}, MPa	Azimuth of S_{Hmax}
ATG_1	Atotsugawa		9.4 (+550)[a]	11.8	3.6	7.8	16.2	7.8	14.6	–2.8	26.1	N42.5°W
ATR_1	Atera	Fukuoka	131.5	12.7	10.1	6.5	8.1	6.5	6.9	5.8	12.4	N22.5°W
ATR_2			243.0	12.9	10.1	8.9	14.2	8.9	6.3	6.6	17.7	(N17.3°E)[b]
ATR_3			263.0	17.3	12.7	9.1	12.0	9.1		11.0	13.7	N17.3°E
ATR_4			269.5	13.1	9.2	8.0	12.1	8.0		6.8	14.6	(N11.7°E)[b]
ATR_5			276.0	14.7	11.0	10.0	16.2	10.0		8.4	18.9	N11.7°E
ATR_6		Hatajiri	249.0	17.1	13.5	11.8	19.4	11.8	12.1	5.0	28.0	(N20.5°W)[b]
ATR_7			258.5	21.4	13.4	12.5	21.5	12.5		9.3	25.7	N20.5°W
ATR_8			266.3	23.3	15.4	14.2	24.5	14.2		11.2	28.8	N8.4°W
ATR_9		Ueno	347.0	14.9	9.0	9.2	15.1	9.2	6.4	8.5	15.7	N3.5°W
RKA_1	Rokko-Awaji	Hirabayashi	307.5	38.1	13.9	11.6	17.8	11.6	9.3	28.8	2.9	N30°W
RKA_2			382.0	13.8	8.3	7.2	9.5	7.2		4.5	13.4	-
RKA_3		Iwaya	627.5	15.4	13.3	10.1	10.7	10.1	16.2	–0.8	25.0	N20°W

[a]Stress measurement was performed in the tunnel at the depth of 550 m.
[b]S_{Hmax} azimuth at the nearest measurement depth is substituted because of the lack of data.

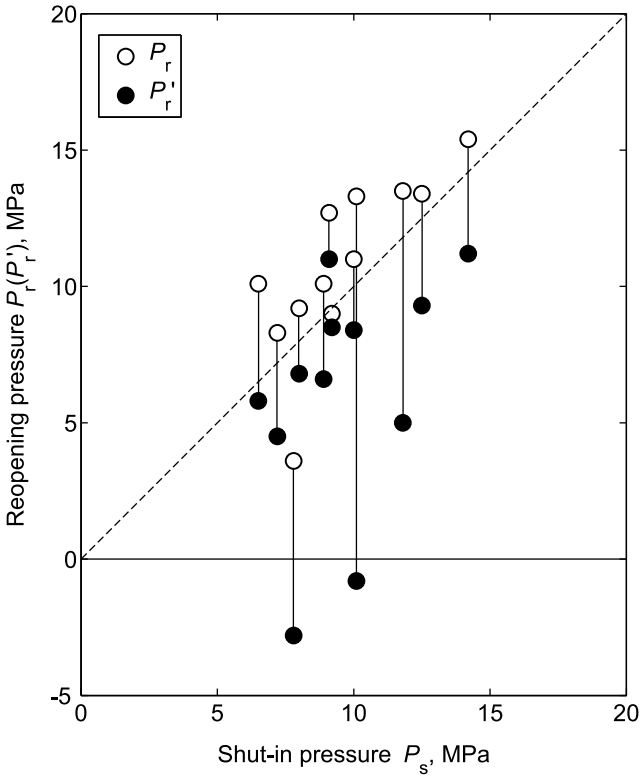

Figure 6. Plot of P_r and P'_r as a function of P_s for 12 data for which both P_r and P'_r are available. The corresponding P_r and P'_r are connected with vertical lines. Data for RKA_1 are not plotted since the in situ measurement seemed to be incorrect. P_r is almost equal to P_s, and all P_r values are greater than P'_r.

the amount of accumulated dislocation can be estimated from the amount of reversal dislocation that returns the decreased r values to the original and uniform values (see Figure 10c). We then determined the amount of left-lateral dislocation on the fault that makes the r values constant at all observation sites independent of the distance from the fault. The calculation was performed with Okada's dislocation model [*Okada*, 1992] using the reestimated stress data shown in Table 5. For simplicity, the fault is assumed to be a rectangular plane with the following geometry: a length of 30 km, a width of 15 km, a strike of N43°W, and a dip of 90°. The assumed fault trace is shown as a dashed line in Figure 8. The slip was also assumed to be a uniform pure left-lateral strike slip. Actually, since we could not find an optimum amount of reversal dislocation that made all r values constant because of possible measurement errors or a nonuniform slip distribution, we adopted the amount of reversal dislocation at which the standard deviation of reconstructed r values was minimized. The amount of right-lateral accumulated dislocation was estimated to be 2.1 m. Figure 11 shows the reconstructed r values calculated from the stress data when the estimated reversal dislocation of 2.1 m on the Atera fault system was applied. The average of the r values was 0.41 ± 0.04. When the coefficients of friction with favorably oriented faults were calculated using the reconstructed stress data, the average coefficient was 0.62 ± 0.06 under the assumption of hydrostatic pore pressure. This quantity is quite consistent with laboratory friction results, such as Byerlee's law [*Byerlee*, 1978]. When and how the right-lateral dislocation was accumulated will be discussed in section 4.

4. Discussion

[17] It should be emphasized that in the calibration test using Inada granite the fracture always occurs along the weakest plane parallel to the core sample axis. This suggests that the tensile strength measured at that location might be underestimated if the anisotropy of the tensile strength is significant compared to the differential stress there. If the tensile strength is anisotropic, the estimation of the orientation of principal stress might be biased in the HFT. However,

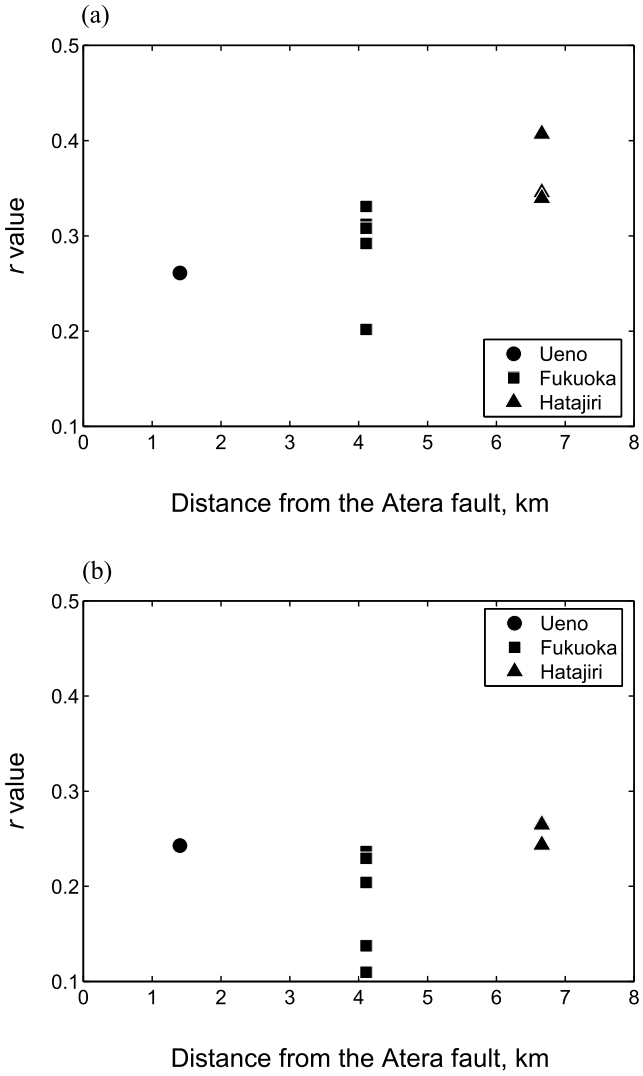

Figure 7. Plot of r values as a function of distance from the Atera fault system. (a) The r values are calculated from the stress data reestimated using the tensile strength of the rocks. The r values, i.e., shear stresses, decrease near the fault. (b) The r values are calculated from the data using the conventional HFT. There seems to be no relation between r values and the distances from the Atera fault system.

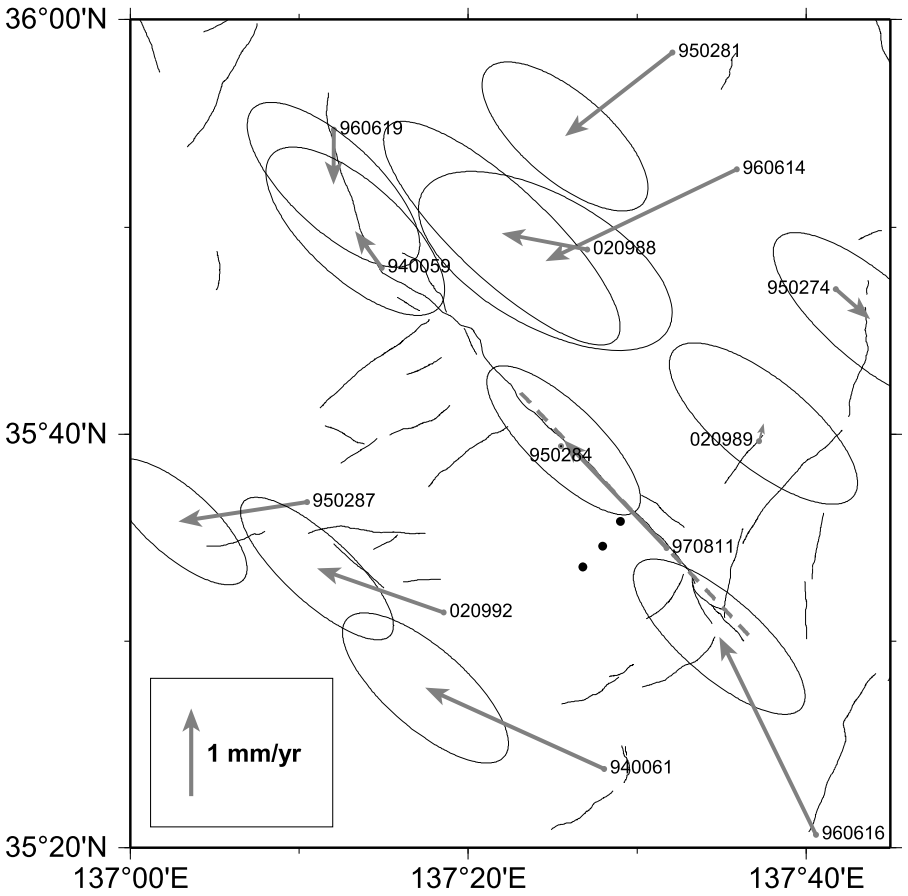

Figure 8. Crustal deformation estimated from the GPS surveys of GEONET by GSI. Arrows show the displacements relative to station 950284. Error ellipses reflect 1σ uncertainty. The southwestern side of the southern segment of the Atera fault system (970811, 020992, 940061, and 960616) seems to move to the northwest in comparison with the northeastern side (020989 and 950274), which means that the fault is dislocating right-laterally. The dashed line is the fault trace assumed for the analysis in section 3.

this problem will become less significant as the depth increases because the differential stress generally becomes large with depth. If we go back to the equation for the stress concentration around a circular hole from *Kirsch* [1898], $\sigma_\theta = 3S_{\mathrm{hmin}} - S_{\mathrm{Hmax}} - 4(S_{\mathrm{hmin}} - S_{\mathrm{Hmax}})\sin^2\theta$, the uncertainty in the orientation is estimated to be ±27° even under stress conditions at the shallowest depth for which data were collected in this study (ATR_1). This uncertainty would not be critical. Here, we assumed the anisotropy of the tensile strength to be 5 MPa based on the data for Inada granite shown in Table 2.

[18] Figure 6 shows the relations among P_s, P_r, and P'_r. We observe that the reopening pressure measured in situ (P_r) is almost equal to the shut-in pressure (P_s) as suggested by *Ito et al.* [1999]. In contrast, the reestimated reopening pressure (P'_r) is apparently different from the corresponding shut-in pressure. It should be noted that P'_r is smaller than P_r except in the data for RKA_1, whose in situ stress measurement might not have been performed successfully. This relationship is also consistent with the finding of *Ito et al.* [1999] that, using the conventional HFT system with large compliance, a slight change in the pressure rate accompanying the reopening of the fracture cannot be detected. Also, the reopening pressure might be overestimated. Overestimating the reopening pressure corresponds to underestimating the horizontal maximum stress (see equation (1)), which would lead to the underestimation of the differential stress and thus the shear stress on a fault. Therefore when the fault strength is discussed based on the in situ stress data [e.g., *Scholz*, 2000; *Townend and Zoback*, 2000], the estimated stress data may lead to an incorrect finding that the fault is weak due to the underestimation of fault strength. Accurate estimation of the reopening pressure can prevent such problems. Accurate estimation of the reopening pressure also enables us to exclude any incorrect stress data that looks plausible; the case of RKA_1 is a good example. Table 5 reveals that S'_{Hmax} (the reestimated horizontal maximum stress) is less than S_{hmin} for RKA_1, though S_{Hmax} (the conventionally estimated horizontal maximum stress) is greater than S_{hmin}. This result contradicts the definition and may be obtained when the in situ HFT procedure has failed; for example, a fracture was accidentally created whose direction is significantly different from the direction of the horizontal maximum stress when the water was pressurized. The fact that the fracture seemed to occur on the fifth pressurization also implies that technical problems occurred (see Figure S10a in auxiliary material).

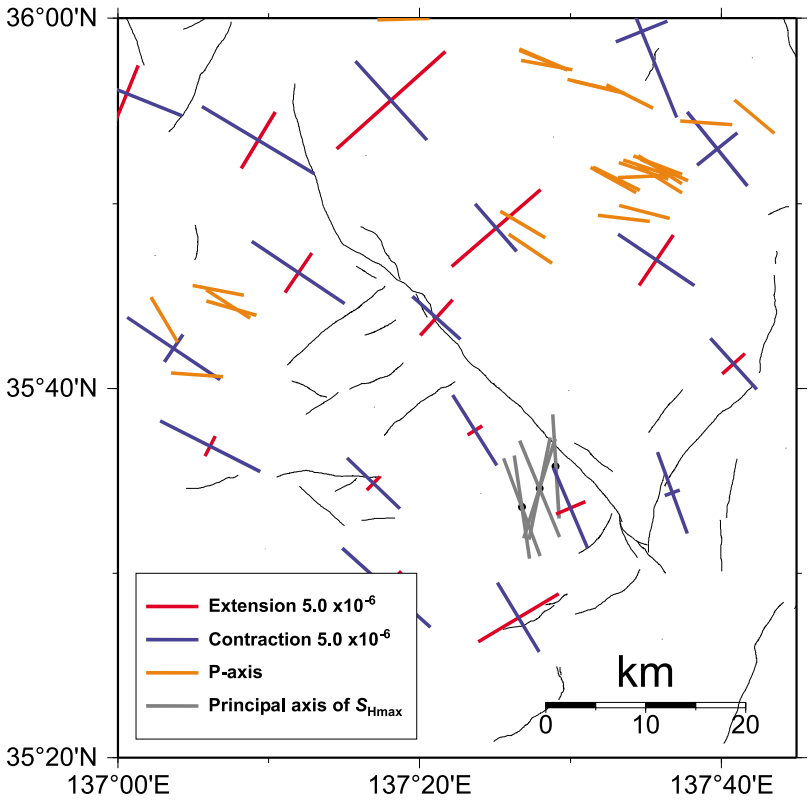

Figure 9. Principal axes of stress and strain around the Atera fault system. Gray lines show the principal axes of horizontal maximum stress estimated from the in situ stress measurement. Crosses with red and blue lines show the strain axes calculated using data from the triangulation survey performed over 102 years by GSI. Red and blue lines represent contraction and extension, respectively. P-axes of earthquakes more than *M*3.5 are shown by orange lines.

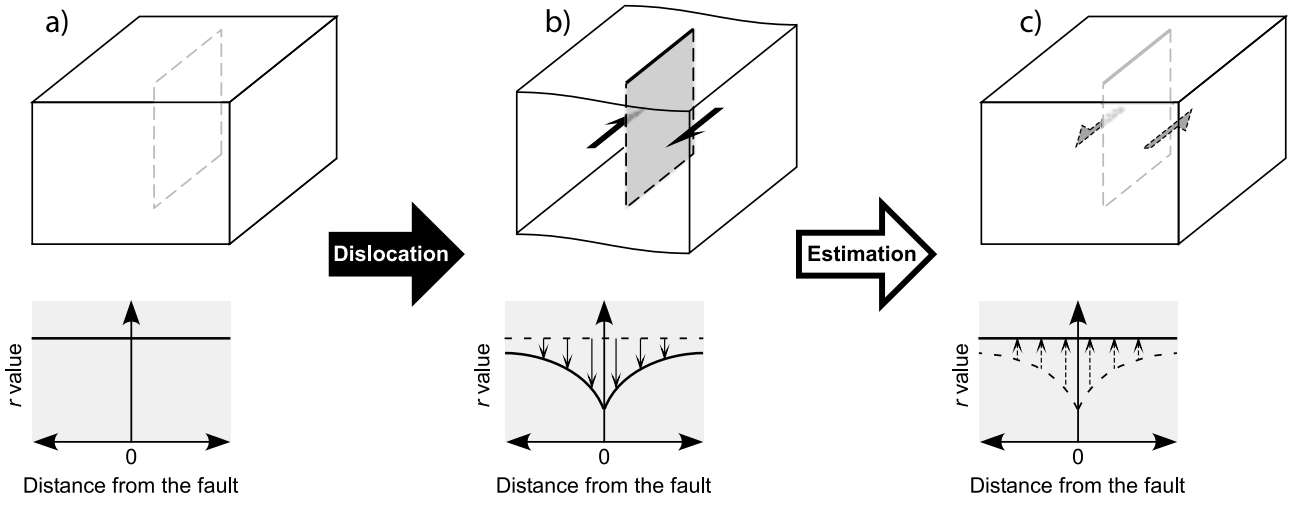

Figure 10. Schematic diagram of the analysis of the Atera fault system including the assumptions and procedures, showing (top) the fault configuration and slip direction at each stage and (bottom) *r* value distribution as a function of distance from the fault. (a) The state after sufficient time has passed since the previous earthquake is shown. The stress field becomes uniform, and thus the *r* values become constant. (b) The state after the dislocation is shown. Shear stress on and around the fault is released, and *r* values decrease near the fault. (c) The reconstructed state obtained by applying the reversal slip is shown.

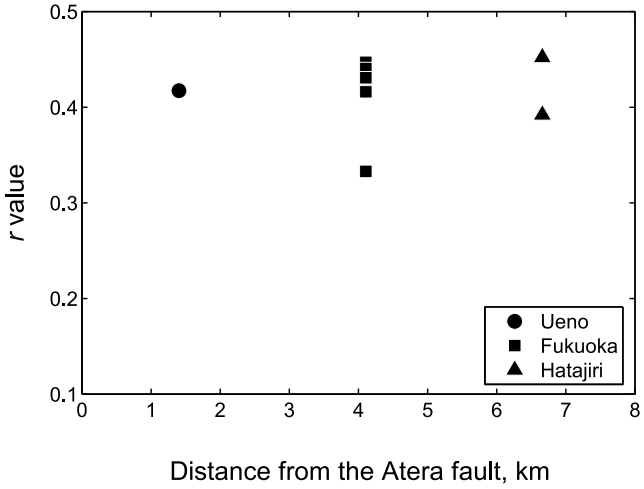

Figure 11. Plot of r value as a function of distance from the Atera fault system. The r values are calculated from the stress data reconstructed by assuming a reversal dislocation so that the r values become constant independent of the distance from the fault.

[19] Although these problems related to the misreading of the reopening pressure may be avoided by using the small compliance HFT system, the problem derived from a negative reopening pressure, as in the data for ATG_1 and RKA_3 in Table 5, remains. As shown in equation (1), the reopening pressure can be negative when S_{hmin} is less than one-third of the sum of S_{Hmax} plus the pore pressure, i.e., when the differential stress is extremely large. In this case, the fracture created by the first pressurization in the HFT will never be closed under such a stress condition. It should be noted that sometimes we cannot estimate the reopening pressure depending on the stress state. Since we do not know the stress state beforehand, we might have to conduct the HFT without knowing. Even in this case, we can estimate the stress value from the breakdown pressure if tensile strength data is available. Consequently, the tensile strength is a very important parameter for accurate and reliable stress estimation using HFT. In particular, there is no way to correct stress data that have been acquired with the large compliance system except by reestimation of the reopening pressure using the tensile strength. The case of the stress data for the Atera fault system is a good example.

[20] The GPS survey seems to reveal that the southern segment of the Atera fault system (the Atera fault) is aseismically dislocating right-laterally at present, whereas geological and geomorphological surveys have indicated that the predominant slip direction was left-lateral in the past. Such a reactivation of the fault with a reversal of the slip direction is known as tectonic inversion and was discovered in the continental crust [e.g., *Jackson*, 1980; *Kim et al.*, 2001]. Other evidence for tectonic inversion has also been discovered in Japan. *Sato* [1994] discussed the historical change in the regional tectonic stress field in northeast Japan based on the observation of dikes, veins, faults orientation, and regional geology. He suggested that the recent activity of the reverse faults in northeast Japan represents the reactivation of the Miocene normal faults. *Maruyama and Lin* [2004] suggested that slip direction inversion occurred in the major active strike-slip faults in southwest Japan based on analyses of deflected river channels, the offset of basement rocks, and fault rock structure. These results indicate that tectonic inversion is a common event in Japan.

[21] However, those inversions of slip direction occurred before several Ma accompanied by a great tectonic event such as the Japan Sea opening, and thus it seems that the case of the Atera fault is not comparable to the tectonic inversions shown above. Therefore it is expected that the Atera fault is under a stress state that easily changes the slip direction of the fault, even if a great tectonic event does not happen. The horizontal strain in Figure 9 represents such features of the stress state around the Atera fault system: the axes of contraction, which can be considered as the axes of maximum compressional stress here, are roughly parallel to the surface trace of the Atera fault, and thus a slight change in the principal axis direction of regional stress will lead to a change in the slip direction. Further evidence for the changeable slip direction can be seen in the investigation by *Sugimura and Matsuda* [1965]. They measured the relative displacements of the river terrace cut by the Atera fault and estimated the displacement vectors from the displacements. Although the vectors demonstrate that the fault type is predominantly left-lateral strike slip, the vectors also show right-lateral strike slip at a certain time after the formation of the terrace, whose age was estimated to be 6030 years B.P. [*Hirano and Nakata*, 1981]. Unfortunately, this right-lateral slip does not agree with the current slip observed by the GPS survey, since the displacement vector shows that vertical and left-lateral strike slips followed the right-lateral slip. This shows that the direction of the slip of the Atera fault has even changed recently, though *Tsukuda et al.* [1993] suggested that the slip direction depends on the location of the reference point of the terrace used for measuring the relative displacement; if the elative displacement by Tsukuda et al. is adopted, the slip direction of the Atera fault becomes left-lateral.

[22] As calculated in section 3, the accumulated right-lateral dislocation was estimated at 2.1 m, which is the amount of slip needed since the time when the stress field was uniform to achieve the present stress distortion near the Atera fault system. The time when the stress field was uniform, in other words, when the fault started to slip right-laterally, can be roughly estimated from the current aseismic slip rate calculated with the GPS data. By averaging the displacement rates at the southern stations (940061, 020992, 970811, 020989, and 950274) projected to the assumed fault plane shown in Figure 8, we estimated a slip rate of 1.9 ± 1.4 mm/yr. This suggests that the total dislocation up to the present-day would have required approximately 1100 ± 800 years to accumulate. Here, it should be noted that this estimation is valid only under the assumption that the slip rate has been constant. The horizontal strain on and in the vicinity of the Atera fault system, which was estimated from the triangulation, is not as distorted as the strain far from the fault, and its value is of the order of 10^{-6} for 102 years; the apparent strain rate estimated from the relative displacement observed by GPS survey, in contrast, is 10^{-7}/yr, i.e., the apparent strain is 10^{-5} for 100 years when using the data of stations 950284, 970811, and 020989. This means that the

estimated aseismic slip may not be steady but might instead be caused by episodic events. Therefore to accumulate the 2.1 m dislocation estimated from the stress data, more than 1100 years are needed, assuming the aseismic slip alone contributes to the accumulation of dislocation. However, it is more reasonable to consider that the dislocation causing the shear stress reduction was mostly caused by the right-lateral dislocation during the previous earthquake because the latest earthquake seems to have occurred only several hundred years ago, as discussed in the next paragraph.

[23] The latest large earthquake in the Atera fault system is considered to be the 1586 Tensho earthquake [*Toda et al.*, 1995]. The Tensho earthquake caused severe damage in a large area in central Japan, and its seismic magnitude is considered to have reached *M*8 [*Iida*, 1987]. *Toda et al.* [1995] conducted a trenching survey at three sites on the Atera fault system and proposed the historical sequence of the faulting events based on the observation of the geological structure of the trenches and the radiocarbon dating of the soil layers. On the basis of the historical sequence and the previous studies of this earthquake in addition to their own results, they determined that the latest seismic faulting in the Atera fault system was between 1400 A.D. and 1600 A.D. Because no earthquakes that caused damage in this area during this period have been reported other than the Tensho earthquake, they concluded that the latest earthquake on the Atera fault system was the 1586 Tensho earthquake. Therefore the Atera fault slipped after 1400 A.D., regardless of whether or not the previous earthquake in the Atera fault system was the Tensho earthquake, and the dislocation seemed to be right-lateral. Unfortunately, since it is quite difficult to determine the direction of the strike slip from only a trenching survey, *Toda et al.* [1995] did not report the slip direction of the faulting.

[24] On the basis of the recent earthquake sequence, *Toda et al.* [1995] also suggested that the probability of the occurrence of the next earthquake in the Atera fault system is low at present because the time lapsed since the Tensho earthquake relative to the average recurrence time is rather short; the ratio of the lapsed time to the recurrence time is only 0.22. Here it should be noted that their estimate was made under the assumption that the Atera fault system has been dislocating left-laterally, but the result found in the present study suggests that this assumption is incorrect. In addition, the earthquake recurrence time in the Atera fault system has fluctuated; in particular, the period from the second-latest event to the latest event has been very short. *Toda et al.* [1995] estimated it to be 593 years at a minimum based on the results of a trenching survey on the Kowachi fault (Figure 4b). Our estimate of 2.1 m dislocation also seems to be small as the coseismic slip of an *M*8 earthquake; since the amount of estimated dislocation includes that of aseismic events, the apparent slip during the latest earthquake becomes further less than mentioned above. This paradox can be resolved if we propose that the Atera fault accumulated some amount of left-lateral dislocation just before the latest earthquake. If this proposition is correct, the apparent amount of dislocation from a neutral point was less than the expected dislocation, though the net amount of actual coseismic dislocation would be much larger. This should also mean that the Atera fault dislocated left-laterally during the second-latest earthquake, and the slip dislocation changed afterward.

[25] In order to explain these unusual characteristics related to the latest earthquake, we here propose a simple hypothetical model of recent seismic cycles in the southern segment of the Atera fault system. Figure 12 shows a schematic diagram of our model. The state of the fault strength and stress field at each stage was as follows.

[26] After sufficient time had passed since the previous earthquake, the fault strength was fully recovered, shear stress accumulated on the fault, and the stress field became uniform with E–W compression (Figure 12a).

[27] The second-latest earthquake occurred left-laterally, which released the shear stress on and around the fault. The fault strength recovered after a sufficient time (Figure 12b).

[28] The N–S compressional tectonic stress increased (or the E–W compression decreased), which resulted in an isotropic stress field and a relative increase in N–S compression near the fault (Figure 12c).

[29] The N–S compressional stress further increased and became dominant in this area. The magnitude of the compressional stress in the N–S direction near the fault became larger than that of the tectonic stress (Figure 12d).

[30] The latest earthquake occurred right-laterally before it would be expected to occur according to the recurrence interval due to the larger stress accumulation near the fault. (Figure 12e) Even if the amount of coseismic slip was similar to that of the previous earthquake, a single earthquake alone may not have been able to completely release the shear stress, since stress in addition to the tectonic stress was accumulated on the fault. Therefore the amount of coseismic slip, evaluated on the basis of the static stress drop relative to the uniform tectonic stress, appears to have been much less than that of most earthquakes.

[31] In order to release the residual shear stress on the fault, right-lateral aseismic slip occurred. (Figure 12f) This model can consistently explain the results of the geological and geophysical observations, though there remain two problems: why the slip direction changed and why the fault strength could not be recovered.

[32] In order to solve these problems, more investigation is needed. First, the distribution of the slip direction and rate over the whole Atera fault system should be clarified. In particular, the stress state of the northern segment seems to be different from that of the southern segment. The aseismic slip also seems to occur only at the southern segment. Dense GPS and SAR surveys will help us understand the present slip activity of the Atera fault system. Investigating the distribution of stress and pore pressure around the fault can greatly contribute to illustrating the physical state of the fault. Detailed seismic observations may make such investigations possible [e.g., *Cornet and Yin*, 1995; *Cornet et al.*, 2007]. In situ stress measurements at greater depths will also provide important information. HFT is a practically unique method of measuring stress at such depths, and thus the tensile strength measurements should be incorporated as shown in this study. Of course, a geological survey is essential for estimating the time and cause of the slip direction change. Investigating the frictional property of the rock and the gouge on the Atera fault plane will lead to a more precise understanding of the conditions under which the fault dis-

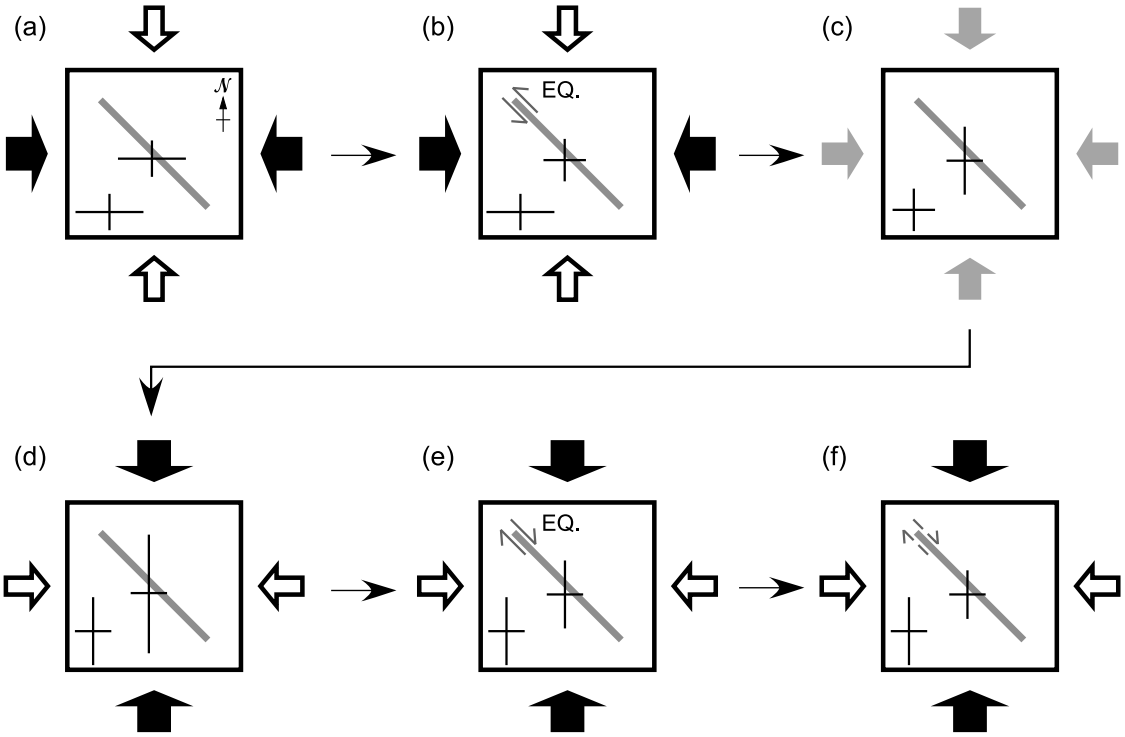

Figure 12. Schematic diagram of a simple hypothetical model of the recent seismic cycle in the southern segment of the Atera fault system. Solid and open arrows represent the tectonic loading. Crosses with solid lines show the relative magnitude of principal stresses in the N–S and E–W directions. The solid black, solid gray, and open arrows represent the largest, middle, and smallest stress magnitudes, respectively. The length of the lines in the cross represents the relative magnitude of the principal stresses. The inclined solid gray line is the simplified fault trace. The stages are as follows: (a) before the second-latest earthquake, (b) occurrence of the second-latest earthquake, (c) change in tectonic stress loading, (d) accumulation of N–S compressional stress, (e) occurrence of the latest earthquake, and (f) aseismic slip after the latest earthquake.

locates aseismically [e.g., *Mizoguchi et al.*, 2007]. Such investigations may help us to understand why the fault cannot recover its strength and the mechanisms of the friction constitutive law.

5. Conclusion

[33] We have developed an apparatus to measure the tensile strength of rock and have confirmed that the tensile strength can be measured reliably with sufficient accuracy using a standard rock sample of Inada granite whose physical properties are well known. We then measured the tensile strength of rock core samples obtained where the HFTs were conducted. We confirmed that the in situ reopening pressure (P_r) is biased as pointed out by *Ito et al.* [1999]. We reestimated the reopening pressure using the tensile strength and reexamined the in situ stress state around the three fault systems (the Atotsugawa, Atera, and Rokko-Awaji fault systems). The reestimated stress data and geodetic data suggest that the southern segment of the Atera fault system is aseismically dislocating right-laterally and that the amount of accumulated dislocation is 2.1 m, though the past dislocation of the Atera fault system has been considered to be left-lateral. While it is still unknown why the slip direction was inverted, the Atera fault changed its slip direction from left-lateral to right-lateral before the latest seismic event.

[34] **Acknowledgments.** Authors would like to thank H. Noda, an anonymous reviewer, Associate Editor, and Editor P. Taylor. Their careful readings of the manuscript and constructive comments were very valuable for revision of the paper. GPS and triangulation survey data were provided by the Geographical Survey Institute of Japan. This study was supported in part by a grant-in-aid from the Core Research for Evolutional Science and Technology (CREST), the Japan Science and Technology Agency.

References

Amadei, B., and O. Stephansson (1997), *Rock Stress and its Measurement*, 490 pp., Chapman and Hall, London.

Brudy, M., M. D. Zoback, K. Fuchs, F. Rummel, and J. Baumgärtner (1997), Estimation of the complete stress tensor to 8 km depth in the KTB scientific drill holes: Implications for crustal strength, *J. Geophys. Res.*, *102*(B8), 18,453–18,475.

Byerlee, J. D. (1978), Friction of rocks, *Pure Appl. Geophys.*, *116*, 615–626, doi:10.1007/BF00876528.

Cornet, F. H., and J. Yin (1995), Analysis of induced seismicity for stress field determination and pore pressure mapping, *Pure Appl. Geophys.*, *145*, 677–700, doi:10.1007/BF00879595.

Cornet, F. H., T. Bérard, and S. Bourouis (2007), How close to failure is a granite rock mass at a 5km depth?, *Int. J. Rock Mech. Min. Sci.*, *44*, 47–66, doi:10.1016/j.ijrmms.2006.04.008.

Cuisiat, F. D., and B. C. Haimson (1992), Scale effects in rock mass stress measurements, *Int. J. Rock Mech. Min. Sci. Geomech. Abstr.*, *29*(2), 99–117, doi:10.1016/0148-9062(92)92121-R.

Fujii, Y., T. Takemura, M. Takahashi, and W. Lin (2007), Surface features of uniaxial tensile fractures and their relation to rock anisotropy in Inada granite, *Int. J. Rock Mech. Min. Sci.*, *44*, 98–107, doi:10.1016/j.ijrmms.2006.05.001.

Haimson, B. C., and F. H. Cornet (2003), ISRM suggested methods for rock stress estimation–Part 3: Hydraulic fracturing (HF) and/or hydraulic testing of pre-existing fractures (HTPF), *Int. J. Rock Mech. Min. Sci.*, *40*, 1011–1020, doi:10.1016/j.ijrmms.2003.08.002.

Haimson, B. C., and Z. Zhao (1991), Effect of borehole size and pressurization rate on hydraulic fracturing breakdown pressure, in *Rock Mechanics Contributions and Challenges: Proceedings of the 31st US Symposium on Rock Mechanics*, edited by W. Hustrulid and G. A. Johnson, pp. 191–199, Taylor and Francis, London.

Hatanaka, Y., T. Iizuka, M. Sawada, A. Yamagiwa, Y. Kikuta, J. M. Johnson, and C. Rocken (2003), Improvement of the analysis strategy of GEONET, *Bull. Geogr. Surv. Inst.*, *49*, 11–37.

Hickman, S., and M. Zoback (2004), Stress orientations and magnitudes in the SAFOD pilot hole, *Geophys. Res. Lett.*, *31*, L15S12, doi:10.1029/2004GL020043.

Hirano, S., and T. Nakata (1981), Prehistoric large earthquakes deduced from fault activities along the Atera fault, central Japan (in Japanese with English abstract), *Geogr. Rev. Jpn.*, *54–5*, 231–246.

Huenges, E., J. Erzinger, J. Kuck, B. Engeser, and W. Kessels (1997), The permeable crust: Geohydraulic properties down to 9101 m depth, *J. Geophys. Res.*, *102*(B8), 18,255–18,266, doi:10.1029/96JB03442.

Iida, K. (1987), *The Record of the Great Tensho Earthquake (in Japanese)*, 552 pp., Nagoya Univ. Press, Nagoya, Japan.

Ikeda, R., Y. Iio, and K. Omura (2001), In situ stress measurements in NIED boreholes in and around the fault zone near the 1995 Hyogo-ken Nanbu earthquake, *Japan, Isl. Arc*, *10*, 252–260, doi:10.1046/j.1440-1738.2001.00323.x.

Ikeda, R., K. Omura, T. Matsuda, Y. Iio (2002), Spatial and temporal variation of in-situ stress in and around active fault zones in central Japan, *Eos Trans. AGU*, *83*(47), Fall Meet. Suppl., Abstract T62C–1338.

Ito, T., K. Evans, K. Kawai, and K. Hayashi (1999), Hydraulic fracture reopening pressure and the estimation of maximum horizontal stress, *Int. J. Rock Mech. Min. Sci.*, *36*, 811–826, doi:10.1016/S0148-9062(99)00053-4.

Jackson, J. A. (1980), Reactivation of basement faults and crustal shortening in orogenic belts, *Nature*, *283*, 343–346, doi:10.1038/283343a0.

Jaeger, J. C., and N. G. W. Cook (1969), *Fundamentals of Rock Mechanics*, 2nd ed., 513 pp, Methuen, London.

Kehle, R. O. (1964), The determination of tectonic stresses through analysis of hydraulic wall fracturing, *J. Geophys. Res.*, *82*, 2018–2026.

Kim, Y.-S., J. R. Andrews, and D. J. Sanderson (2001), Reactivated strike-slip faults: Examples from north Cornwall, UK, *Tectonophysics*, *340*, 173–194, doi:10.1016/S0040-1951(01)00146-9.

Kirsch, G. (1898), Die Theorie der Elastizitat und die Bedurfnisse der Festigkeitslehre, *Z. Ver. Dtsch. Ing.*, *42*, 797–807.

Lee, M. Y., and B. C. Haimson (1989), Statistical evaluation of hydraulic fracturing stress measurement parameters, *Int. J. Mech. Min. Sci. Geomech. Abstr.*, *26*, 447–456, doi:10.1016/0148-9062(89)91420-4.

Lin, W. (2002), Permanent strain of thermal expansion and thermally induced microcracking in Inada granite, *J. Geophys. Res.*, *107*(B10), 2215, doi:10.1029/2001JB000648.

Lin, W., M. Takahashi, T. Nakamura, and Y. Fujii (2008), Tensile strength and deformability of Inada granite and their anisotropy: Comparison between uniaxial tension and Brazilian test (in Japanese with English abstract), *Jiban Kogaku Janaru*, *3*(2), 165–173, doi:10.3208/jgs.3.165.

Lund, B., and Z. D. Zoback (1999), Orientation and magnitude of in situ stress to 6.5 km depth in the Baltic Shield, *Int. J. Rock Mech. Min. Sci.*, *36*, 169–190, doi:10.1016/S0148-9062(98)00183-1.

Maruyama, T., and A. Lin (2004), Slip sense inversion on active strike-slip faults in southwest Japan and its implications for Cenozoic tectonic evolution, *Tectonophysics*, *383*, 45–70, doi:10.1016/j.tecto.2004.02.007.

Mizoguchi, K., E. Fukuyama, K. Kitamura, M. Takahashi, K. Masuda, and K. Omura (2007), Depth-dependent strength of the fault gouge at the Atotsugawa fault, central Japan: A possible mechanism for its creeping motion, *Phys. Earth Planet. Inter.*, *161*, 115–125, doi:10.1016/j.pepi.2007.01.003.

Okada, Y. (1992), Internal deformation due to shear and tensile faults in a half-space, *Bull. Seismol. Soc. Am.*, *82*, 1018–1040.

Sano, O., H. Ito, A. Hirata, and Y. Mizuta (2005), Review of methods of measuring stress and its variations, *Bull. Earthquake Res. Inst. Univ. Tokyo*, *80*, 87–103.

Sato, H. (1994), The relationship between late Cenozoic tectonic events and stress field and basin development in northeast Japan, *J. Geophys. Res.*, *99*(B11), 22,261–22,274, doi:10.1029/94JB00854.

Schmitt, D. R., and M. D. Zoback (1989), Poroelastic effects in the determination of the maximum horizontal principal stress in hydraulic fracturing tests - A proposed breakdown equation employing a modified effective stress relation for tensile failure, *Int. J. Rock Mech. Min. Sci. Geomech. Abstr.*, *26*(6), 499–506.

Scholz, C. H. (2000), Evidence for a strong San Andreas fault, *Geology*, *28*(2), 163–166, doi:10.1130/0091-7613(2000)28<163:EFASSA>2.0.CO;2.

Sugimura, A., and T. Matsuda (1965), Atera fault and its displacement vectors, *Geol. Soc. Am. Bull.*, *76*, 509–522, doi:10.1130/0016-7606(1965)76[509:AFAIDV]2.0.CO;2.

Takemura, T., and M. Oda (2005), Changes in crack density and wave velocity in association with crack growth in triaxial tests of Inada granite, *J. Geophys. Res.*, *110*, B05401, doi:10.1029/2004JB003395.

Toda, S., D. Inoue, A. Kubouchi, N. Takase, and M. Nikaido (1995), Paleoseismicity of the Atera fault system and 1586 Tensho earthquake: Trenching studies at Ogo, Aonohara and Dendahara, central Japan (in Japanese with English abstract), *Zisin*, *48*, 401–421.

Toda, S., D. Inoue, and K. Miyakoshi (1996), Paleoseismicity of the Atera fault system, central Japan, during the Holocene (part 2) -Fault activity of the northern part and segmentation model, *Rep. U95060*, 42 pp., Cent. Res. Inst. of Electr. Power Indust., Tokyo.

Townend, J., and M. D. Zoback (2000), How faulting keeps the crust strong, *Geology*, *28*(5), 399–402, doi:10.1130/0091-7613(2000)28<399:HFKTCS>2.0.CO;2.

Townend, J., and M. D. Zoback (2004), Regional tectonic stress near the San Andreas fault in central and southern California, *Geophys. Res. Lett.*, *31*, L15S11, doi:10.1029/2003GL018918.

Tsukuda, E., Y. Awata, H. Yamazaki, Y. Sugiyama, K. Shimokawa, and K. Mizuno (1993), Explanatory text of the strip map of the Atera Fault system (in Japanese with English abstract), *Tecton. Map Ser. 7*, 39 pp., scale 1:25,000, Geol. Surv. of Jpn., Tsukuba, Japan.

Yamashita, F., E. Fukuyama, and K. Omura (2004), Estimation of fault strength: Reconstruction of stress before the 1995 Kobe earthquake, *Science*, *306*, 261–263, doi:10.1126/science.1101771.

Zoback, M. L. (1992), First- and second-order patterns of stress in the lishosphere: The world stress map project, *J. Geophys. Res.*, *97*(B8), 11,703–11,728, doi:10.1029/92JB00132.

E. Fukuyama, K. Mizoguchi, K. Omura, and F. Yamashita, National Research Institute for Earth Science and Disaster Prevention, Tennodai, Tsukuba, Ibaraki 305-0006, Japan. (yamafuto@bosai.go.jp)